Critical Phenomena in Neutron Stars II: Head-on Collisions

Thorsten Kellerman[1], **Luciano Rezzolla**[1,2] **and David Radice**[1]

[1] Max-Planck-Institut für Gravitationsphysik, Albert Einstein Institut, Potsdam, Germany
[2] Department of Physics and Astronomy, Louisiana State University, Baton Rouge, USA

Abstract. We consider the head-on collision of equal-mass neutron stars boosted towards each other and we study the behavior of such systems near the threshold of black-hole formation. In particular, we confirm the previous findings by [1] that a type-I critical phenomenon can be observed by fine-tuning the initial mass of the two neutron stars. At the same time, we argue against the interpretation that the critical solution is not a perturbed spherical star and show instead that the metastable star corresponds to a (perturbed) equilibrium solution on the unstable branch of the equilibrium configurations. As a result, the head-on collision of two neutron stars near the critical threshold can be seen as a transition in the space of configurations from an initial stable solution over to a critical metastable one which can either migrate to a stable solution or collapse to a black hole. The critical exponent for this process shows a fine structure which was already observed in the case of the critical collapse of scalar fields but never before for perfect fluids.

PACS numbers: 04.25.Dm, 04.40.Dg, 04.70.Bw, 95.30.Lz, 97.60.Jd

1. Motivation and introduction

In 1993, Choptuik [2] considered one-parameter families of solutions, $\mathcal{S}[P]$, of the Einstein-Klein-Gordon equations for a massless scalar field in spherical symmetry, such that for every $P > P^\star$, $\mathcal{S}[P]$ contains a black hole and for every $P < P^\star$, $\mathcal{S}[P]$ is a solution not containing singularities. He studied numerically the behavior of $\mathcal{S}[P]$ as $P \to P^\star$ and found that the critical solution, $\mathcal{S}[P^\star]$, is *universal*, in the sense that it is approached by all nearly-critical solutions regardless of the particular family of initial data considered. He also found that $\mathcal{S}[P]$ exhibit discrete self-similarity and that, for supercritical solutions ($P > P^\star$), the mass of the black hole satisfies $M_{\rm BH} = c|P-P^\star|^\gamma$, with γ being an universal constant, *i.e.* not depending on the particular family of initial data.

After Choptuik's seminal work, similar transitions were discovered for a wide range of systems, including massive scalar fields and ultra-relativistic fluids, see [3] for a recent review. All these phenomena have the common property that, as P approaches $P^\star$, $\mathcal{S}[P]$ approaches a universal solution $\mathcal{S}[P^\star]$ and that all the physical quantities of $\mathcal{S}[P]$ depend only on $|P - P^\star|$. In analogy with critical phase transitions in statistical mechanics, these transitions in gravitational collapse were later classified as "type-I" critical phenomena, with static or periodic critical solutions and discontinuous transitions in the vicinity of the critical point, or "type-II" critical phenomena, with self-similar critical solutions and continuous transitions in the vicinity of the critical solution [3].

The study of critical phenomena in neutron-star (NS) collapse started with the work by [4] on radiation fluids and was later extended to more general ultra-relativistic equations of state (EOS) [5,6] and ideal-gas EOS [7–9]. In all these studies the collapse was triggered using strong perturbations and a type-II critical phenomena was found. Type-I critical phenomena

in the collapse of unstable configuration under very small perturbations was instead studied only very recently [10, 11].

The first study of critical phenomena the head-on collision of NSs was instead carried out by Jin and Suen in 2007 [1]. In particular, they considered a series of families of equal mass NSs, modeled with an ideal-gas EOS, boosted towards each other and varied the mass of the stars, their separation, velocity and the polytropic index in the EOS. In this way they could observe a critical phenomenon of type I near the threshold of black-hole formation, with the putative solution being a nonlinearly oscillating star. In a successive work [12], they performed similar simulations but considering the head-on collision of Gaussian distributions of matter. Also in this case they found the appearance of type-I critical behaviour, but also performed a perturbative analysis of the initial distributions of matter and of the merged object. Because of the considerable difference found in the eigenfrequencies in the two cases, they concluded that the critical solution does not represent a system near equilibrium and in particular not a perturbed Tolmann-Oppenheimer-Volkoff (TOV) solution [1].

In this paper we study the dynamics of the head-on collision of two equal-mass NSs using a setup which is as similar as possible to the one considered in [1]. While we confirm that the merged object exhibits a type-I critical behaviour, we also argue against the conclusion that the critical solution cannot be described in terms of equilibrium solution. Indeed, we show that, in analogy with what found in [11], the critical solution is effectively a perturbed unstable solution of the TOV equations. Our analysis also considers fine-structure of the scaling relation of type-I critical phenomena and we show that it exhibits oscillations in a similar way to the one studied in the context of scalar-field critical collapse [13, 14].

The remainder of this paper is organized as follows. In section 2 we describe the numerical settings of the simulations, the properties of the used initial data and we define some of the quantities that we analysed. In section 3 we show in details our results, while section 4 is dedicated to conclusions and discussion. Finally, presented in Appendix A is a study of the compactness of the metastable solution and a comparison with its "hoop radius". The work reported is closely related to the analysis carried in a companion paper (hereafter paper I) about critical phenomena in linearly unstable nonrotating NS models [11]. Because of the logical affinity between the two works we will often refer the reader to the results obtained in [11]. We use a spacelike signature $(-,+,+,+)$, with Greek indices running from 0 to 3, Latin indices from 1 to 3 and the standard convention for the summation over repeated indices. Unless explicitly stated, all the quantities are expressed in the system of dimensionless units in which $c = G = M_\odot = 1$.

2. Numerical setup and initial models

In what follows we briefly describe the numerical setup used in the simulations and the procedure followed in the construction of the initial data.

2.1. Numerical Setup

The numerical setup used in our simulations is identical to the one presented in [11]. In particular, we use the axisymmetric code `Whisky2D`, which has been described in detail in [15] (but see also the more extended discussion in paper I) and is based on the 3-dimensional code `Whisky` [16–18], to solve in 2 spatial dimensions the full set of Einstein and relativistic-hydrodynamics equations. The axisymmetry of the spacetime is imposed exploiting the "cartoon" technique introduced in [19], while the hydrodynamics equations (which are written

in first-order form and thus do not require double spatial derivatives) are written explicitly in cylindrical coordinates (see [15] to read about the advantages of this formulation).

All the simulations presented here have been performed using an ideal-gas EOS, $p = (\Gamma - 1)\rho\epsilon$, where ρ is the baryonic density and ϵ the specific internal energy in the rest frame of the fluid‡. The discretization of the spacetime evolution equations is done using fourth-order finite-differencing schemes, while we high-resolution shock-capturing (HRSC) methods with a piecewise-parabolic method (PPM) reconstruction for the hydrodynamics equations. The time-stepping is done with a third-order total-variation diminishing (TVD) Runge-Kutta scheme and despite the use of higher-order methods, the convergence order drops to about 1 after the two NSs have merged and large shocks develop (see [20] for a discussion on the convergence order in relativistic-hydrodynamics simulations).

The spatial discretization is done a grid with uniform resolution, which we have taken to be either $h = 0.1\ M_\odot$ or $h = 0.08\ M_\odot$. Furthermore, as long as nonspinning NSs are considered, the head-on collision also possesses a symmetry across the plane midway between the two stars and orthogonal to the colliding direction. As a result, the problem needs to be solved only for one star and suitable boundary conditions be applied across the symmetry plane. The outer boundary of the computational domain is set at $60\ M_\odot$ and thus rather close to the two stars. However, this is adequate since we are not interested here in extracting gravitational waveforms and since we have verified that the violation of the constraints at the outer boundaries are not larger than elsewhere in the computational domain.

As a final remark we note that we use the same gauges as those employed in [21] and thus the slicing is sufficiently "singularity-avoiding" that it is not necessary to perform an excision of the field variables when following the evolution of a supercritical solution. However, because of the very high-resolution used, the rapid growth of the rest-mass density is not compensated by the intrinsic numerical dissipation as instead happens in [21] or in [18]. As result we excise the solution of the hydrodynamical quantities only as discussed in [17, 22] in order to obtain a stable, long-term solution.

2.2. Initial data

Our initial data consists of two equal-mass nonrotating NSs having initial coordinate separation, computed as the coordinate distance between the two stellar centres, of $20\ M_\odot$. Following [1], we construct these stars using a polytropic EOS, $p = K\rho^\Gamma$, with adiabatic exponent $\Gamma = 2$ and polytropic constant $K = 80$, which is equivalent to $K = 0.00298\, c^2/\rho_{\rm n}$, and where $\rho_{\rm n} = 2.3 \times 10^{14}\ {\rm g/cm}^3$ is approximately the nuclear density. The stars in the neighbourhood of the critical solution have a radius of $R = 14.7$ km, a baryon/gravitational (ADM) mass of $0.760/0.732\ M_\odot$. The main properties of the critical solution are reported in table 1, where they are indicated as model "A".

Note that the maximum baryon/gravitational mass for the chosen value of the polytropic constant is $1.609/1.464\ M_\odot$ and thus the object produced by the collision will have a baryon/gravitational mass which is above such maximum mass. However, as we will discuss below and in contrast with the claim made in [1], this can still lead to equilibrium solution for a TOV star.

The stars constructed in this way are then boosted towards each other along the z-axis with a velocity $v_0 = 0.15$, which is similar to the free-fall velocity as computed from the Newtonian expression for a point-particle. With these choices the only remaining free parameter needed to characterize the initial data is the central rest-mass density of the two

‡ We recall that an ideal-gas EOS and a polytropic one are identical for fluids undergoing isoentropic evolutions.

Table 1. Equilibrium models used for the collision (model A) or that are discussed in figure 5 (models B and C). Listed are: the value of the gravitational (ADM) mass, the total rest-mass, the radius of the star, the central rest-mass density and the polytropic constant K. For each model we also report the maximum allowed ADM and rest-masses for a TOV having the same polytropic constant.

Model	$M_{\rm ADM}$	M_b	R (km)	ρ_c	K	$M_{\rm ADM,max}$	$M_{b,\rm max}$
A	0.732	0.760	14.761	0.00058	80	1.464	1.609
B	1.505	1.514	9.135	0.00963	145	1.972	2.166
C	1.460	1.547	19.003	0.00055	155	2.038	2.240

NSs, ρ_c, which we use as our critical parameter (We note that the value chosen for the initial velocity does influence qualitatively the results obtained and indeed it can act as a critical parameter in a sequence at constant ρ_c [1]).

2.3. Entropy of the critical solution

A convenient way to study the properties of the critical solution is to characterize its thermodynamical properties and in particular its entropy. The basic idea is that the metastable (critical) solution is simply an equilibrium solution on the unstable branch of TOV configurations and thus that by measuring its entropy it is possible to relate it to the corresponding equilibrium polytropic model. Following [23], we express the second law of thermodynamics as

$$S \,=\, S_0 \,+\, C_{\rm V}\ \ln(T) \,-\, R\ \ln(\rho), \tag{1}$$

where S_0 is an integration constant that we set to zero and where

$$C_{\rm V} \,=\, \left(\frac{d\epsilon}{dT}\right)_{\rm v} \tag{2}$$

is the specific heat capacity at constant pressure. and R the gas constant. In the case of an ideal gas R is related to the specific heat capacities through the relation

$$R \,=\, C_{\rm p} \,-\, C_{\rm V} \,=\, \left(\frac{dh}{dT}\right)_{\rm p} - \left(\frac{d\epsilon}{dT}\right)_{\rm v}, \tag{3}$$

where $h = 1 + \epsilon + p/\rho$ is the specific enthalpy. Recalling that $\epsilon = C_{\rm V} T$ and $\Gamma = C_{\rm p}/C_{\rm V}$, the second law of thermodynamics (1) for a polytropic EOS is simply given by

$$S \,=\, C_{\rm V}\ \ln\left(\frac{K}{C_{\rm V}(\Gamma-1)}\right), \tag{4}$$

or equivalently

$$K \,=\, R\ \exp\left(\frac{S}{C_{\rm V}}\right). \tag{5}$$

Stated differently, the polytropic constant reflects all of the changes in the entropy of the system, so that expression (5) allows a simple connection between the entropy of the critical solution, which we measure as proportional to $K = p/\rho^{\Gamma}$, and the properties of a corresponding equilibrium TOV model.

In practice the polytropic constant can change enormously across the star especially after the collision and since we are interested only in global quantities we use a volume-averaged polytropic constant

$$\langle K \rangle \, = \, \frac{\int_\Omega p/\rho^\Gamma dV}{\int_\Omega dV}, \tag{6}$$

and perform the volume integration not across the whole star but over a volume Ω where the rest-mass density is larger than 10% of the initial central one. This choice removes the difficulties with possible divergences near the stellar surface and we have verified that is robust against different values of the threshold density.

3. Results

We next discuss the dynamics of the collision and the properties of the critical solution as they appear from our numerical simulations.

3.1. Dynamics of the collision

The basic dynamics of the process is rather simple to describe. As the two NSs are accelerated towards each other by the initial boost and the mutual gravitational attraction, they collide, leading to a merged object which is wildly oscillating and with a mass which is above the maximum mass of the initial configuration. Depending on whether the initial central density is larger or smaller than the critical one, the metastable solution either collapses to a black hole (supercritical solutions) or it expands to a new stable stellar solution (subcritical solutions).

Before entering the details of the discussion it may be useful to remark that the simulation of the head-on collision of two NSs in the neighborhood of the critical solution is a very demanding calculation, even for modern general-relativistic hydrodynamical codes. This is because adaptive mesh refinements do not provide any significant speed up and, at the same time, rather high level of resolutions are needed to capture the dynamics faithfully. In spite of these computational difficulties mentioned above, using the `Whisky2D` code we are able to identify the critical value for ρ_c with an accuracy of 11 significant digits, a level of precision never achieved before in the study of NS head-on collisions. More specifically, we have measured the critical central density

$$\rho_c^\star = (5.790998966725 \pm 0.00000000003) \times 10^{-4}. \tag{7}$$

as the midpoint between the largest central rest-mass density among the subcritical models and the smallest central rest-mass density among the supercritical ones. In other words, binaries with $\rho_c > \rho_c^\star$ have been simulated to collapse to a black hole, while binaries with $\rho_c < \rho_c^\star$ have been computed to expand to a stable star.

As pointed out by [1], this value will ultimately depend on the numerical resolution used and the other discretization parameters. Nevertheless, given a set of initial data and numerical setup, (7) gives a precise measure of how close we are able to get to the critical solution.

Compressed in figure 1 is a considerable amount of information about the criticality of the head-on collision. More specifically, we show the time evolution of the central rest-mass density of the heaviest subcritical model (black solid line) and lightest supercritical model (red dashed line) computed. Overall, we can distinguish three different phases of the dynamics. In the first one (marked with "A" in the figure) the central density increases from its initial value to a maximum one reached, which is attained when the stellar cores merge.

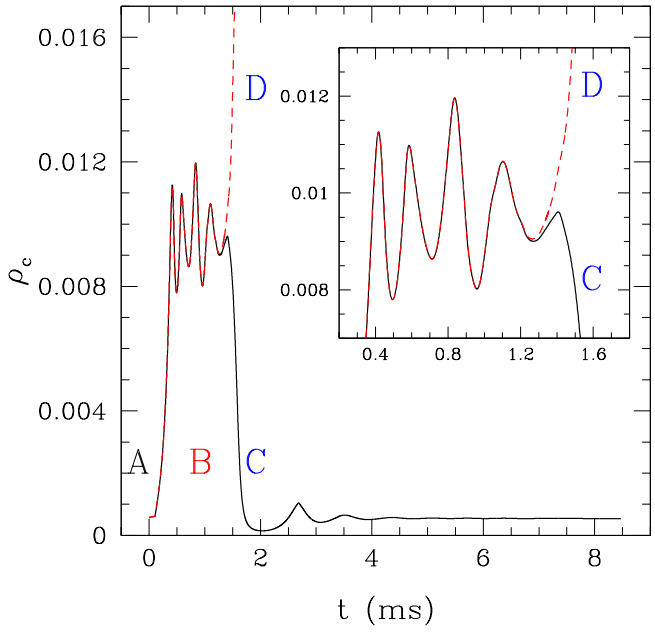

Figure 1. Evolution of the maximum rest-mass density of the most massive subcritical model with initial value $\rho_c = 0.000579099896670$ (black solid line) the least massive supercritical model with initial value $\rho_c = 0.000579099896675$ (red dashed line). Also highlighted are the four different phases of the dynamics. The first one corresponds to the initial configuration of the system (labelled as "A"). After the collision, a new metastable solution is created during which the central density exhibits violent oscillations (labelled as "B"); the subrcritical and supercritical solutions are essentially indistinguishable during this stage. Finally the subcritical and supercritical solutions separate, with the first one relaxing to a stable expanded configuration (labelled as "C"), while the second collapses to a black hole (labelled as "D").

The second phase (marked with "B") starts from $t \sim 0.4$ ms and is characterized by strong oscillations around the metastable equilibrium. During these first two phases the subcritical solution d the supercritical one are essentially indistinguishable, but at the end of the second phase, *i.e.* at $t \sim 1.2$ ms, the different nature of the two solutions emerges and the evolutions of the rest-mass density differ. More specifically, during the third phase (marked with "C" and "D"), the supercritical solution shows an exponential increase of the central rest-mass density as a result of the collapse to a black hole. The subcritical solution, on the other hand, shows a violent expansion and the central density settles to a value which is about one tenth of the maximum one attained during the second phase. Clearly, the most interesting part is obviously the one corresponding to the second phase, during which the merged object is a metastable solution in which the central density has strong, non-harmonic oscillations (see inset of figure 1).

In order to better describe the dynamics of the system, we show in figures 2 and 3 the evolution of colour-coded countours of the rest-mass density of the supercritical and subcritical solutions, respectively, when shown at representative times in the (x, z) plane. The first row of panels in figure 2 shows the initial configuration of the system at time $t = 0$ and a subsequent stage, at time $t = 0.394$ ms, corresponding to when the first maximum in the rest-

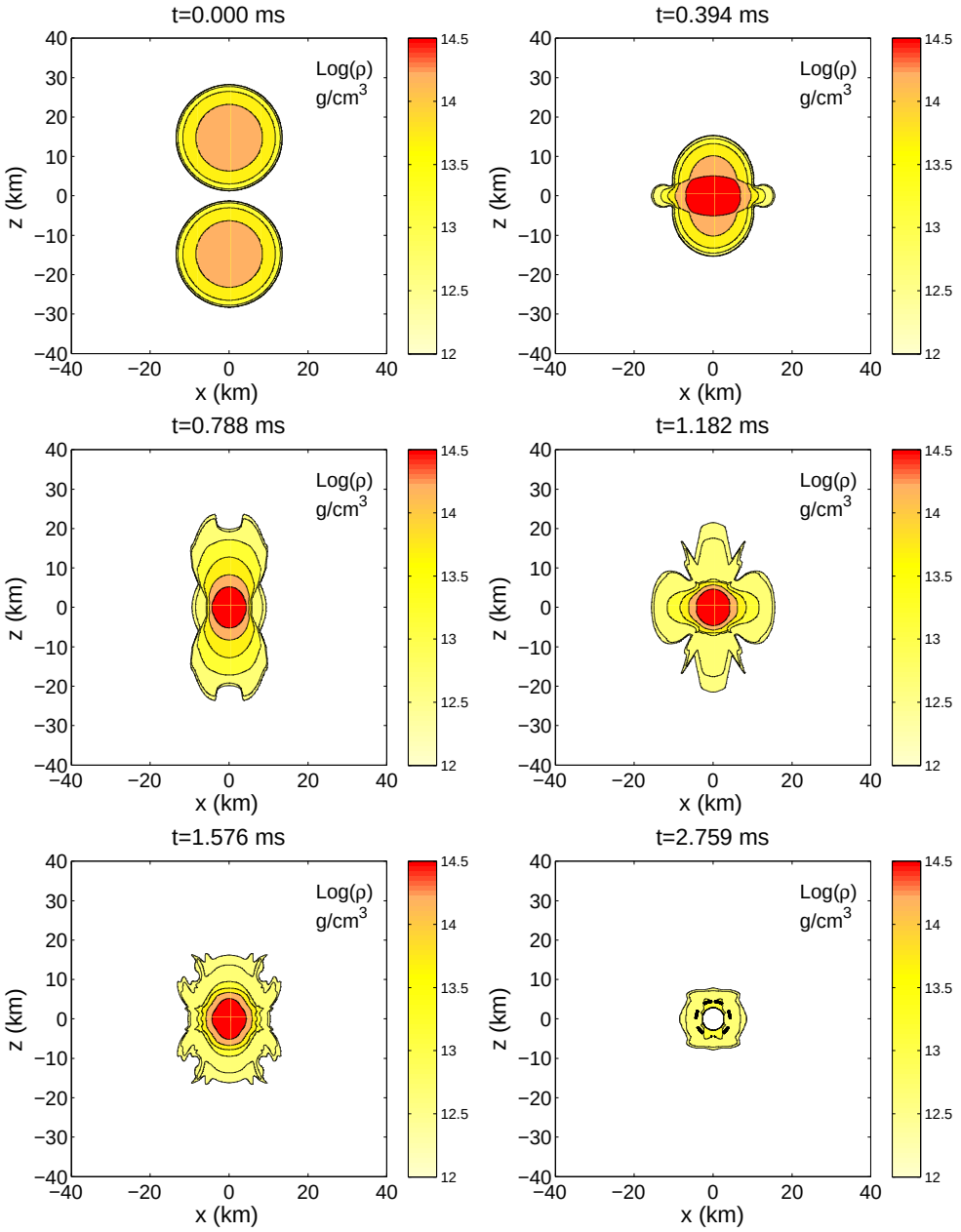

Figure 2. Isodensity contours in the (x, z) plane of the least massive supercritical solution ($\rho_c = 0.000579099896675$). The corresponding times are shown at of each panel, while the color-code for the rest-mass density is indicated to the right. The isolines are shown for the values of $\rho = 10^{12.6}, 10^{12.7}, 10^{13.2}, 10^{13.7}, 10^{14.2}$ and $10^{14.7}$ g/cm^3. The second frame ($t = 0.394$ ms) is taken during the merge process. The next five frames illustrate the star during the metastable equilibrium. Finally the last frame ($t = 2.759$ ms) shows the solution after the formation of a black hole, whose apparent horizon is shown with a thick black dashed line.

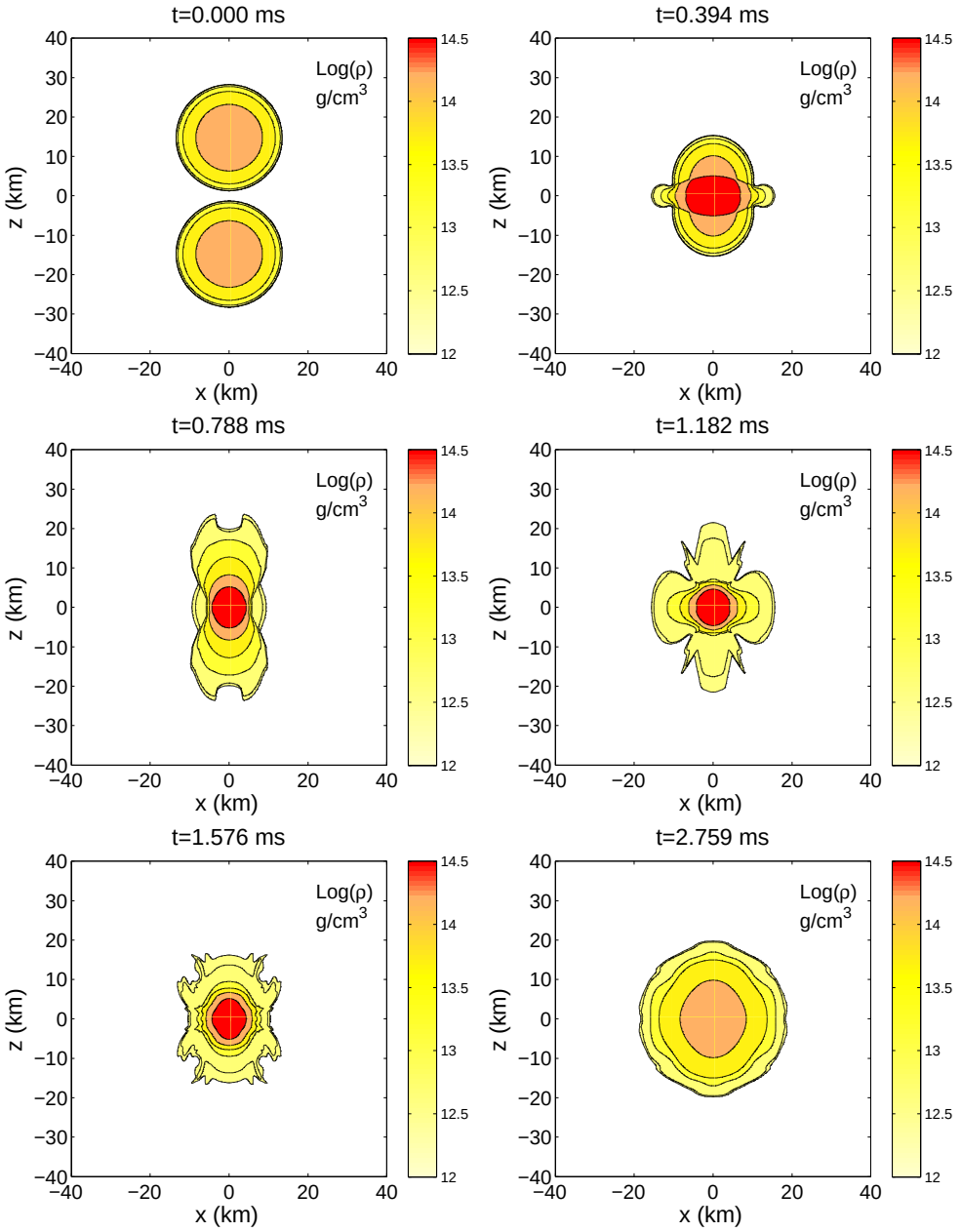

Figure 3. The same as figure 2, but for the most massive subcritical model ($\rho_c = 0.000579099896670$). The first five frames are similar (although not identical) to the corresponding ones in figure 2 since they refer to the metastable evolution when the two solutions are essentially indistinguishable. The last frame ($t = 2.759$ ms) shows a new NS produced from the migration of the metastable object to the stable branch of the equilibrium solutions.

mass density is reached (*cf.* figure 1). This time also represents the one at which the two stellar cores enter in contact and thus marks the beginning of the metastable equilibrium. During this stage, two strong shock waves propagate along the z-direction, ejecting part of the matter as shown in the third panel at time $t = 0.788$ ms. Most of this matter is still gravitationally bound and falls back onto the central object creating a new shock wave (*cf.* fourth panel at $t = 1.182$ ms). This process is then repeated multiple times and results in a sequence of bounces until the object finally collapses to a black hole, as shown in the last panel at time $t = 2.759$ ms and which marks the fate of the supercritical solution.

Similarly, figure 3, reports representative stages of the evolution of the subcritical solution. A rapid inspection of the first five panels of figure 2 indicates they are very similar to the corresponding ones in figure 2. Indeed, the supercritical and subcritical solutions are the same to the precision at which we measure the critical solution [*cf.* (7)] and we have reported the panels here exactly to remark the similarity during the first two stages of the evolution. However, being it a subcritical solution, the metastable evolution does not end with a black hole formation but, rather, with a new stable stellar solution. This is shown in the sixth panel of figure 3 and refers to a time $t = 2.759$ ms, after the metastable star has expanded violently and when it has reached a new quasi-spherical configuration.

With the exception that we are able to get closer to the critical solution, much of what reported here confirms what found by Jin and Suen in [1]. In the following section, however, we discuss how and why our conclusions about the properties of the critical solutions differ from those discussed in [1] and subsequently in [12].

3.2. Nearly-critical solutions

The scope of this section is to show that, contrary to what suggested in [1, 12], the metastable object can be interpreted rather simply as the perturbation of a new equilibrium configurations of linearly unstable spherical stars. To provide evidence that this is the case, we have computed the evolution of the average entropy of the system for a subcritical solution as computed via the volume-averaged polytropic constant (6). This is shown in figure 4, where we report both $\langle K \rangle$ and the central density ρ_c during the metastable equilibrium or stage "B" (left panel) and when the metastable solution has expanded to recover a stable solution or stage "3" (right panel).

Clearly, the two panels show that two quantities are correlated and indeed in phase opposition – entropy increases when the density decreases and viceversa – as one would expect from the first law of thermodynamics

$$TdS = pdV + dQ = pdV \,, \tag{8}$$

where the second equality comes from assuming adiabatic transformations.

Using the results shown in figure 4, it is then possible to compute a time-averaged value of $\langle K \rangle$ and of the central density, *i.e.* $\overline{\langle K \rangle}$, $\overline{\rho_c}$, and thus equilibrium polytropic models with such polytropic constant and central density. These equilibrium models can be constructed either relative to the metastable stage or relative to the final stable stage of the subcritical solutions.

The results of this procedure are summarized in figure 5, which reports the equilibrium sequences of TOV stars with fixed polytropic constant in a standard $(\rho_c, M_{\rm ADM})$ plane. In particular, the black solid line refers to a sequence with $K = 80$ and the black triangle therefore marks the initial critical solution (*i.e.* model "A" in table 1). Similarly, the red long-dashed line refers to a sequence with a polytropic constant $\overline{\langle K \rangle} = 145$, which therefore coincides with the time averaged value of K during the metastable state and as deduced from

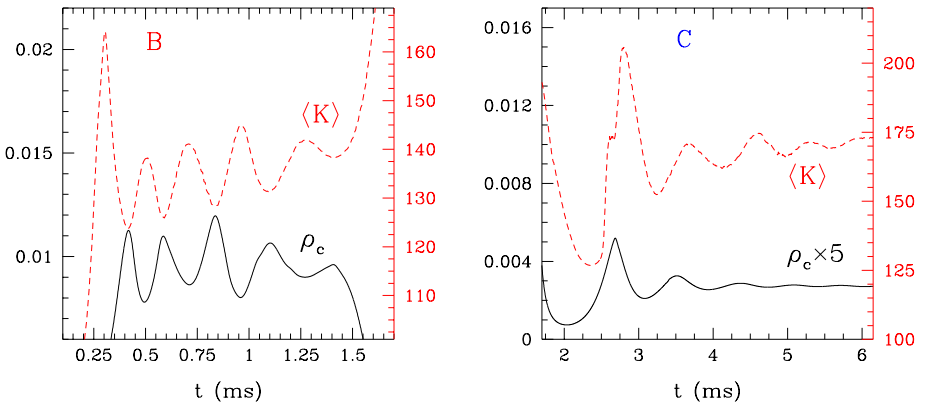

Figure 4. *Left panel:* Evolution of the central rest-mass density and of the effective polytropic constant $\langle K \rangle$ for the most massive subcritical model during the metastable equilibrium phase of the dynamics. *Right panel:* The same as in the left panel but during the relaxation to a stable configuration.

figure 4. The red square shows therefore the equilibrium model having as central density the time-averaged central density of the metastable solution (*i.e.* model "B" in table 1). Finally, the blue dashed line refers to a sequence with a polytropic constant $\overline{\langle K \rangle} = 155$, which therefore coincides with the time averaged value of K during the stable stage of the subcritical solutions. (*cf.*figure 4). The blue pentagon shows therefore the equilibrium model having as central density the time-averaged central density of the stable solution (*i.e.* model "C" in table 1). It is important to remark that because models "A, B, C" are determined after fixing the polytropic constant and the central rest-mass density, they are not guaranteed to have the same total baryon mass. In practice, however, they do have the same rest-mass with a precision of 0.4% (of course $2M_{b,A} \simeq M_{b,B} \simeq M_{b,C}$). This is not a coincidence but a clear evidence of the common link among the three models.

What is eloquently shown in figure 5 can also be stated summarized as follows. The head-on collision of two NSs near the critical threshold can be seen as series of transitions in the space of configurations from an initial stable model "A" over to a metastable model "B" which has the same rest-mass but larger gravitational mass as a result of the conversion of the kinetic energy into internal energy via large shocks. Because model "B" is on the linearly unstable branch of the equilibrium configurations, it can exhibit a critical behaviour (this was shown in great detail in paper I) and thus subcritical solutions will expand and move the stable branch of equilibrium solutions (model "C"), while supercritical solutions will collapse to a black hole (solution "D").

In the light of this interpretation, the conclusion drawn by Jin and Suen [1] that the merged object is far from being a TOV because it promptly collapses even though its total rest-mass is smaller than the corresponding maximum mass, does not appear to be the correct one. Indeed, the transition highlighted in figure 5 clearly shows that even a sub-massive TOV can be brought over the stability threshold to collapse to black hole by simply increasing its gravitational mass, namely by increasing its internal energy.

Additional evidence that the merged object is indeed a perturbed TOV comes from analyzing the oscillation frequencies measured over the metastable stage. Despite the latter is rather short and the eigenfrequencies are consequently not very accurate, they agree well

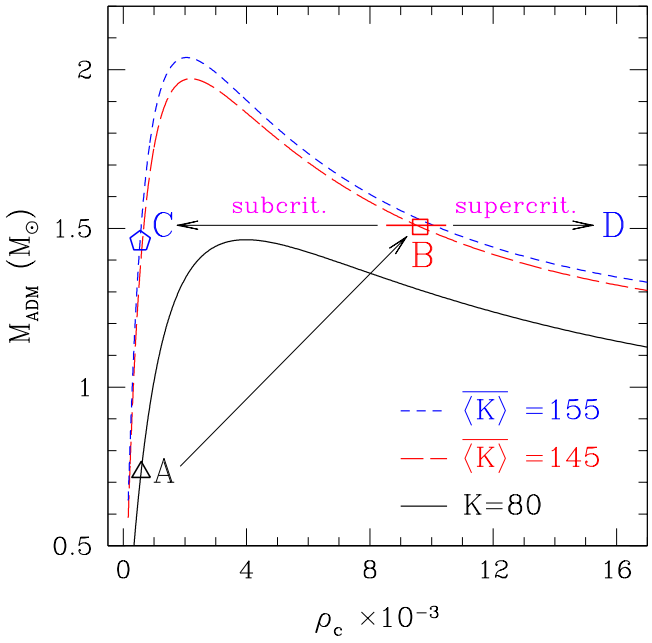

Figure 5. Equilibrium sequences of TOV stars with fixed polytropic constant in a standard $(\rho_c, M_{\rm ADM})$ plane. The black solid line refers to a sequence with $K = 80$ and the black triangle marks the initial critical solution (*i.e.* model "A" in table 1). The red long-dashed line to a sequence with $\overline{\langle K \rangle} = 145$ and the red square shows the equilibrium model having as central density the time-averaged central density of the metastable solution (*i.e.* model "B" in table 1). Finally, the blue dashed line refers to a sequence with $\overline{\langle K \rangle} = 155$ and the blue pentagon shows the equilibrium model having as central density the time-averaged central density of the stable solution (*i.e.* model "C" in table 1). All models "A, B, C" have the same rest-mass to a precision of 0.4% and the arrows show how the collision corresponds to a number of transition in the space of configurations.

with the ones obtained from the linear perturbation theory for the corresponding TOV model. This is reported in table 2, which collects the oscillation frequencies as computed from a Fourier analysis of the central rest-mass density of the largest subcritical solution. Because these frequencies with their error-bars are within the expected ones, we cannot confirm the claim made in [12] that the frequencies of the critical solution are 1 or 2 orders of magnitude smaller than the corresponding equilibrium ones. Rather, we conclude that the metastable critical solution is indeed only a perturbed TOV star.

3.3. On the critical exponent and its fluctuations

The theory of critical phenomena predicts a precise scaling relation between the survival time of the nearly-critical solutions, namely the time over which a metastable equilibrium exists, and the distance from the critical solution. At lowest order this scaling relation is a simple power-law of the type

$$\tau_{\rm eq} \simeq -\gamma \ln |\rho_c - \rho_c^\star| + \text{const}\,. \tag{9}$$

Following [1], we measure the survival time by considering the function $\zeta(t) = (\alpha - \alpha^\star)/\alpha^\star$, where α is the lapse function at the coordinate origin of a given simulation and $\alpha^\star$ is

Table 2. Eigenfrequencies of the modes of the critical solution during the metastable phase of the dynamics as computed from the evolution of the the central rest-mass density. Also indicated are the first overtones of the fundamental mode for a TOV star constructed with K and ρ_c equal to the time-averages of $\langle K \rangle$ and $\langle \rho_c \rangle$ during the metastable phase. Despite the large uncertainty due to the very short integration time, the match between the two set of eigenfrequencies is very good.

Mode	Observed freq. (kHz)	TOV freq. (kHz)
H1	4.8 ± 1.2	3.95
H2	7.2 ± 1.2	6.86
H3	9.6 ± 1.2	9.42
H4	12.0 ± 1.2	11.85

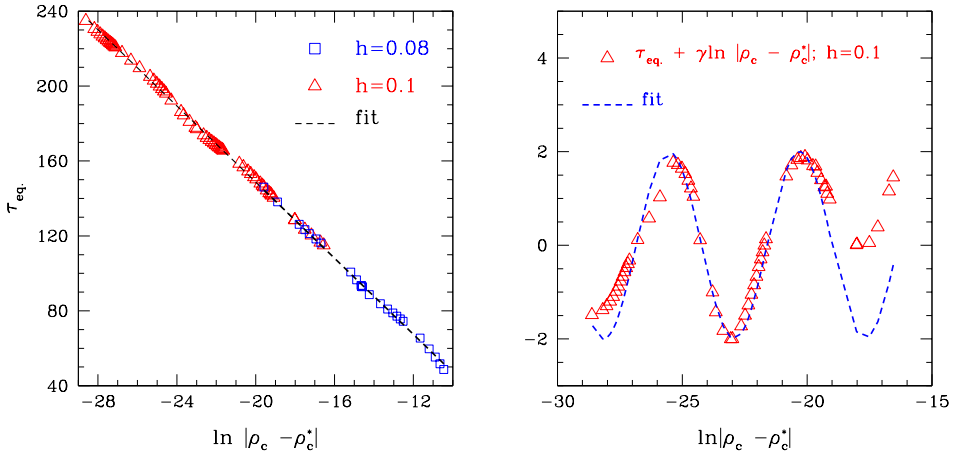

Figure 6. *Left panel:* Survival time of the metastable solution plotted against the logarithm of the difference between the initial central density of the stars and the critical one. The red triangles represent the data points obtained with a grid resolution of $h = 0.1$ and the blue squares represent the ones obtained with $h = 0.08$. The black dashed line represents the expected power-law scaling. *Right panel:* Harmonic fluctuations in the critical exponent γ as obtained after subtracting the power-law scaling from the data points computed with $h = 0.1$ (red triangles). Indicated with a blue dashed line is the fitting sine function.

the lapse of the best numerical approximation of the critical solution. We set $\tau_{\rm eq}$ to be the first (coordinate) time at which $\zeta(\tau_{\rm eq}) \geq 0.05$; as discussed in [1], the determination of the critical exponent does not depend sensitively on this cut-off time. Finally, we compute γ performing a linear least-square fit of (9) on the data points. The results of this process are shown in the left panel of figure 6, where we report with red triangles the values of $\tau_{\rm eq}$ as computed from about 60 simulations having different initial central density. As we will discuss below, such a large number of data points is necessary not only to measure accurately the exponent γ, but also to determine whether nonlinear corrections to expression (9) should be considered. In this way we have computed the critical exponent to be $\gamma = 10.004$, which agrees within 8.4%, with the value computed by [1]. As a further validation, we have computed the critical exponent also for a (smaller) set of simulations carried out at a higher resolution (*i.e.* $h = 0.08$ vs $h = 0.1$) and these are shown as blue squares. These higher-resolution simulations predict a critical exponent of 10.303, thus with a difference of 2.9% from the lower-resolution ones.

A more careful analysis of the data for the survival time reveals that relation (9) is well reproduced by the data, but also that the latter show additional, fine-structure features which are are not accounted for in (9). In particular, it is apparent already at a visual inspection that the critical exponent also shows a periodic change as the solution approaches the critical one. This is highlighted in the right panel of figure 6, where we show the deviations of the data from the relation (9), and where it is apparent that these deviations are essentially harmonic in the range in which data is available (for simplicity and to increase the precision of the fit, we have considered only the low-resolution data, for which more simulations are available). As a result, we can correct the scaling relation (9) with a simple expression of the type

$$\tau_{\rm eq} \simeq -\gamma \ln |\rho_c - \rho_c^\star| + c_1 \sin\left(c_2 \ln |\rho_c - \rho_c^\star| + c_3\right) + \text{const}\,. \tag{10}$$

where $c_1 \simeq 2.0$, $c_2 \simeq 1.2$ and $c_3 \simeq 0.8$. Interestingly, this fine structure of the time-scaling relation has been observed also in in the critical collapse of scalar fields [13, 14], but has never been reported before for perfect fluids, although it may be present also in the data of [1] (*cf.* their figure 4). Because the scaling relation (9) is derived after performing a linear analysis near the critical solution [5], the additional oscillation captured in expression (10) is a purely nonlinear effect which has not been yet fully explained.

4. Conclusions

Critical phenomena are ubiquitous in many different branches of physics and are of great interest in general relativity where they are associated with phase transition of families of solutions. With the goal of studying the occurrence of type-I critical collapse, we considered the head-on collision of equal mass, nonrotating NSs boosted towards each other. After fixing the initial velocity of the stars, we evolved numerically a great number of configurations with different initial central rest-mass density using the 2D general relativistic hydrodynamical code `Whisky2D`.

Overall, the basic dynamics of the process is rather simple: As the two NSs are accelerate towards each other, they collide leading to a merged object which is wildly oscillating and with a gravitational mass which is above the maximum mass of the initial configuration. Depending on whether the initial central rest-mass density is larger or smaller than the critical one, the metastable solution either collapses to a black hole (supercritical solutions) or expands to a new stable stellar solution (subcritical solutions). Exploiting the accuracy of the code and the large set of initial configurations considered, we were able we are able to identify the critical value for the central density with an accuracy of 11 significant digits, a level of precision never achieved before in this type of study.

Although overall more accurate, much of the results reported here about the critical behaviour coincide and confirm those found by Jin and Suen in [1, 12]. However, we do differ and significantly when it comes to the interpretation of the critical solutions. More specifically we have shown that the head-on collision of two NSs near the critical threshold can be seen as series of transitions in the space of configurations from an initial stable model over to a metastable one with the same rest-mass but larger gravitational mass as a result of the conversion of the kinetic energy into internal energy via large shocks. The metastable solution is on the linearly unstable branch of the equilibrium configurations and thus it can exhibit a critical behaviour (see paper I) and either move the stable branch of equilibria (subcritical solutions), or will collapse to a black hole (supercritical solutions). Hence, the critical solution is indeed a (perturbed) TOV solution, in contrast with the conclusions drawn in [1, 12]

Finally, we have also computed the critical exponent of the scaling relation of type-I critical phenomena and found it to agree well with the one computed by [1]. However, we

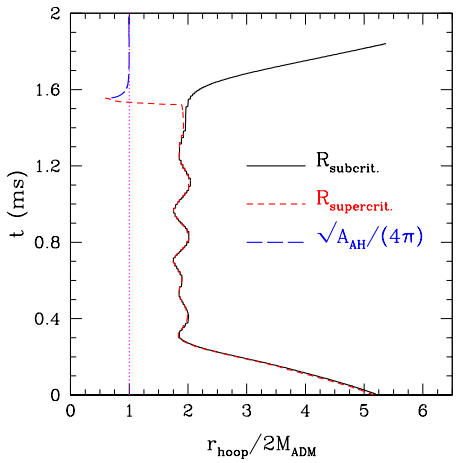

Figure A1. Spacetime diagram showing the worldines of the proper stellar radius for either a subcritical solution $R_{\rm subcrit.}$ (black solid line) or for a supercritical solution $R_{\rm supercrit.}$ (red dashed line). Both quantities are expressed in units of twice the ADM mass, so that the vertical dotted line at 1 represents the threshold below which the hoop conjecture would be violated (the time coordinate is the proper time of an observer comoving at R). Also indicated with a blue long-dashed line is the worldline of the apparent horizon which is relevant in the case of the supercritical solution. Note that the metastable solution is always outside its "hoop".

have also found that, superimposed with the standard power-law, the scaling law shows a fine structure in terms of a periodic fluctuation. These wiggles in the critical exponent have already been observed in the case of type-II critical collapse of massless scalar fields [13, 14], but were never reported before in the case of perfect fluids.

Acknowledgments

It is a pleasure to thank Bruno Giacomazzo and Filippo Galeazzi for their help and assistance with the `Whisky2D` code. We are also grateful to Shin'ichiro Yoshida for useful discussions. This work was supported in part by the IMPRS on "Gravitational-Wave Astronomy", by the DFG grant SFB/Transregio 7, and by "CompStar", a Research Networking Programme of the European Science Foundation. The computations were performed on the Damiana cluster at the AEI.

Appendix A. Metastable solutions and the hoop conjecture

As discussed in the main text, near the critical solution and during the metastable stage, the evolution of all the hydrodynamical and field variables is essentially the same (to a precision which is proportional to the distance from the critical solution) for both subcritical and supercritical solutions. It is therefore natural to ask whether the metastable solution, which can either produce a black hole or an expanded star, is ever compact enough to violate the hoop conjecture. We recall that the conjecture states that a black hole is formed if and only if a "mass" M of matter is confined in a hoop of radius which is in every direction is smaller or equal to the corresponding Schwarzschild radius. Stated differently, a black hole is expected to form if the matter is enclosed in a hoop of proper circumference $\mathcal{C} \leq 4\pi M$.

The hoop conjecture, as it was originally formulated, is not meant to be a precise mathematical statement [24], even though it can be made precise under particular circumstances [25–27]. Most importantly, it is meant mostly as a qualitative description of the gravitational collapse due to the compression of matter. In particular the conjecture leaves much freedom in the definition of both $\mathcal{C}$ and M. In view of this freedom, we have taken $\mathcal{C}$ to be the proper circumference of a coordinate circle enclosing $95\ \%$ of the mass of the system (in order to exclude the extended low-density regions) and used the ADM mass within $\mathcal{C}$ as a local measure of the mass (This use of the ADM mass is strictly speaking incorrect as such a mass is well defined only at spatial infinity; however it provides an approximation which is adequate for the quality of the arguments made here).

In figure A1 we show in a spacetime diagram the worldlines of the proper stellar radius for either a subcritical solution $R_{\rm subcrit.}$ (black solid line) or for a supercritical solution $R_{\rm supercrit.}$ (red dashed line). Both quantities are expressed in units of twice the ADM mass, so that the vertical dotted line at 1 represents the threshold below which the hoop conjecture would be violated (the time coordinate is the proper time of an observer comoving at R). Also indicated with a blue long-dashed line is the worldline of the apparent horizon which is relevant in the case of the supercritical solution. Quite clearly the metastable solution is always outside its "hoop" (indeed about twice as large) and when the supercritical solution crosses it is to produce a black hole as the conjecture predicts. It remains unclear how these worldlines would evolve if we had considered stars with larger boosts or that are are far from the critical solution. These questions will be addressed in our future work on the subject.

As a final remark we note that if we had used the interpretation of the head-on collision as a transition between a stable and a metastable TOV solution (*i.e.* the one summarized in figure 5), then it would have been rather obvious that the hoop conjecture cannot be violated: a TOV star has a surface which is always outside of its Schwarzschild radius.

References

[1] Jin K J, Suen W M and et al 2007 *Phys. Rev. Lett* **98** 131101
[2] Choptuik M W 1993 *Phys. Rev. Lett.* **70** 9
[3] Gundlach C and Martín-García J 2007 *Living Reviews in Relativity* **10** 5
[4] Evans C R and Coleman J S 1994 *Phys. Rev. Lett.* **72** 1782–1785
[5] Hara T, Koike T and Adachi S 1996 *ArXiv General Relativity and Quantum Cosmology e-prints* (*Preprint* `arXiv:gr-qc/9607010`)
[6] Brady P, Choptuik M, Gundlach C and Neilsen D 2002 *Class. Quantum Grav.* **19** 6359–6375
[7] Novak J 2001 *Astron. Astrophys.* **376** 606 (*Preprint* `gr-qc/0107045v1`)
[8] Noble S C 2003 *A Numerical Study of Relativistic Fluid Collapse* Ph.D. thesis University of Texas at Austin (*Preprint* `gr-qc/0310116v1`)
[9] Noble S C and Choptuik M W 2008 *Physical Review D* **78** 064059 (*Preprint* `0709.3527`)
[10] Liebling S L, Lehner L, Neilsen D and Palenzuela C 2010 Evolutions of magnetized and rotating neutron stars (*Preprint* `1001.0575v1`)
[11] Radice D, Rezzolla L and Kellerman T 2010 *Classical and Quantum Gravity submitted*
[12] Wan M B, Jin K J and Suen W M 2008 Dynamical analysis of the structure of neutron star critical collapses (Preprint `0807.1710v2`)
[13] Gundlach C 1997 Phys. Rev. D **55** *695 (Preprint `gr-qc/9604019`)*
[14] Hod S and Piran T 1997 Physical Review D **55** *440 (Preprint `arXiv:gr-qc/9606087`)*
[15] Kellerman T, Baiotti L, Giacomazzo B and Rezzolla L 2008 Classical and Quantum Gravity **25** *225007 (Preprint `0811.0938`)*
[16] Baiotti L, Hawke I, Montero P J, Löffler F, Rezzolla L, Stergioulas N, Font J A and Seidel E 2005 Phys. Rev. D **71** *024035 (Preprint `gr-qc/0403029`)*
[17] Giacomazzo B and Rezzolla L 2007 Class. Quantum Grav. **24** *S235 (Preprint `gr-qc/0701109`)*
[18] Baiotti L, Giacomazzo B and Rezzolla L 2008 Phys. Rev. D **78** *084033 (Preprint `ArXive-prints0804.0594`)*

[19] Alcubierre M, Brandt S R, Brügmann B, Holz D, Seidel E, Takahashi R and Thornburg J 2001 Int. J. Mod. Phys. D **10** *273–289 (Preprint gr-qc/9908012)*
[20] Baiotti L, Giacomazzo B and Rezzolla L 2009 Class. Quantum Grav. **26** *114005 (Preprint 0901.4955)*
[21] Baiotti L and Rezzolla L 2006 Phys. Rev. Lett. **97** *141101 (Preprint gr-qc/0608113)*
[22] Hawke I, Löffler F and Nerozzi A 2005 Phys. Rev. D **71** *104006 (Preprint gr-qc/0501054)*
[23] Chandrasekhar S 1939 An introduction to the study of stellar structure *(New Haven, USA: Dover Publications)*
[24] Wald R M 1997 Gravitational collapse and cosmic censorship (Preprint gr-qc/9710068v3)
[25] Flanagan E 1991 Phys. Rev. D **44** *2409–2420*
[26] Senovilla J M M 2008 Europhysics Letters **81** *20004 (Preprint 0709.0695v3)*
[27] Schoen R and Yau S T 1983 Communications in Mathematical Physics **90** *575–579*